Icarus xxx (2012) xxx–xxx

Contents lists available at SciVerse ScienceDirect

Icarus

journal homepage: www.elsevier.com/locate/icarus

Weakening of ice by magnesium perchlorate hydrate

Hendrik J. Lenferink [a], William B. Durham [a,*], Laura A. Stern [b], Asmin V. Pathare [c]

[a] Massachusetts Institute of Technology, 77 Massachusetts Ave., Cambridge, MA 02139, United States
[b] U.S. Geological Survey, 345 Middlefield Road, Menlo Park, CA 94025, United States
[c] Planetary Science Institute, 1700 E. Fort Lowell, Tucson, AZ 85719, United States

ARTICLE INFO

Article history:
Available online xxxx

Keywords:
Mars, Polar caps
Ices
Ices, Mechanical properties

ABSTRACT

We show that perchlorate hydrates, which have been detected at high circumpolar martian latitudes, have a dramatic effect upon the rheological behavior of polycrystalline water ice under conditions applicable to the North Polar Layered Deposits (NPLD). We conducted subsolidus creep tests on mixtures of ice and magnesium perchlorate hydrate, $Mg(ClO_4)_2{\cdot}6H_2O$ (MP6), of 0.02, 0.05, 0.10, and 0.47 volume fraction MP6. We found these mixtures to be increasingly weak with increasing MP6 content. For mixtures with $\leqslant$0.10 volume fraction MP6, we resolved a stress exponent of $n \approx 2$ at low stresses transitioning to $n \approx 4$ above 10 MPa. Scanning electron microscopy of deformed specimens revealed MP6 to be distributed as an interconnected film between ice grains. These results suggest that grain boundary sliding (GBS) may be enhanced with respect to pure ice. As the enhancement of GBS is expected in polycrystalline aggregates containing a few percent melt or otherwise weak material distributed along grain boundaries, the observed $n \approx 2$ is consistent with the mutual accommodation of basal slip and GBS. If ice containing trace concentrations of MP6 is also much weaker than pure ice at low stresses, flow in the NPLD could be significantly enhanced, particularly at the warmer basal temperatures associated with higher martian obliquities.

1. Introduction

The Phoenix Mars Lander detected 0.4–0.6% perchlorate by mass in martian soils located at high northern latitudes (Hecht et al., 2009). Considering the ubiquity of terrestrial perchlorate (ClO_4^-) within the Antarctic Dry Valleys (Kounaves et al., 2010), perchlorate is likely to be widespread in the martian polar regions. If the North Polar Layered Deposits (NPLD)—the largest surface reservoir of actively-exchanging water ice on Mars—contain a few percent dust (Langevin et al., 2005) with a perchlorate component similar to that observed at the Phoenix landing site, the effects of this phase may be sufficient to enhance flow rates in the NPLD. For example, Fisher et al. (2010) suggested that perchlorate brines in basal layers could indirectly facilitate flow in the overlying NPLD. In this work, we investigate the direct rheological effects of perchlorate upon polycrystalline ice deforming at martian polar temperatures.

The ice plus magnesium perchlorate ($Mg(ClO_4)_2$) system is of particular interest. This system has a eutectic melting temperature (T_e) of 206 K at 56 wt.% H_2O (Fig. 1), where the two phases are ice I and $Mg(ClO_4)_2{\cdot}6H_2O$, or "MP6" (Chevrier et al., 2009; Pestova et al., 2005). More recently Stillman and Grimm (2011a) reported T_e = 216 K based on dielectric permittivity measurements. Although Hecht et al. (2009) detected a variety of cations at the Phoenix landing site (in order of descending concentration: Mg^{2+}, Na^+, Ca^{+2}, K^+), the predominant form of perchlorate should be MP6, based on its stability at low temperatures (Robertson and Bish, 2011).

The occurrence of a eutectic in icy systems generally means that at near-eutectic compositions and temperatures, the solid is weaker than pure ice. There are clear examples of such behavior in icy systems containing ammonia (Durham et al., 1993) and NaCl (De La Chapelle et al., 1995). The weakening effect in the ice-MP6 system may be especially pronounced, given that the depth of eutectic melting with respect to the melting temperatures of the two end-member phases is so large (Fig. 1). To test this hypothesis and quantify the effect, we conducted a series of deformation experiments on ice containing various concentrations of MP6.

2. Flow of icy systems exhibiting a eutectic

Steady-state rheological behavior can be described by the constitutive relationship (e.g., Poirier, 1985)

$$\dot{\varepsilon} = A\sigma^n d^{-p} \exp\left(-\frac{E^* + PV^*}{RT}\right). \quad (1)$$

* Corresponding author.
E-mail addresses: hendrik@mit.edu (H.J. Lenferink), wbdurham@mit.edu (W.B. Durham), lstern@usgs.gov (L.A. Stern), pathare@psi.edu (A.V. Pathare).

0019-1035/$ - see front matter © 2012 Elsevier Inc. All rights reserved.
http://dx.doi.org/10.1016/j.icarus.2012.09.028

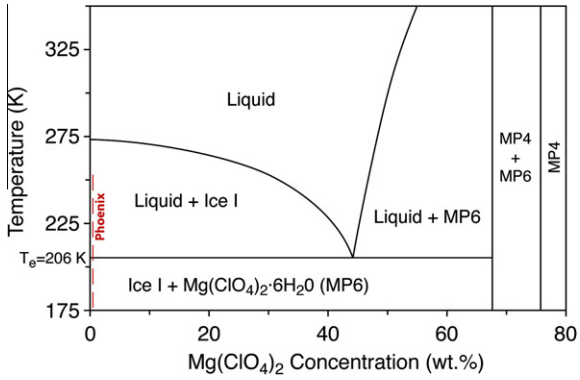

Fig. 1. A portion of the phase diagram for the system H_2O–$Mg(ClO_4)_2$, after Chevrier et al. (2009). The vertical red dashed line indicates estimated MP6 concentration near 0.5 wt.% (Hecht et al., 2009) and measured soil temperature range at the Phoenix Mars Lander site 175–253 K (Zent et al., 2010). (For interpretation of the references to color in this figure legend, the reader is referred to the web version of this article.)

Here $\dot{\varepsilon}$ is strain rate, σ is differential stress (simply referred to as stress), d is grain size, P is pressure, T is absolute temperature, R is the universal gas constant, and A, n, p, E^*, and V^* are constants specific to the material and to the deformation mechanism. Several mechanisms of deformation have been observed in pure polycrystalline ice (Table 1). Deformation in the laboratory of coarse-grained, pure ice is generally carried out and rate limited by dislocation creep, with grains changing shape through intracrystalline plasticity and accompanied by recrystallization. For ice at martian temperatures, grain size-sensitive mechanisms such as diffusional flow and grain boundary sliding (GBS) play an important role at low stresses. Diffusional flow, both within grain interiors as well as along grain boundaries, is expected on a theoretical basis (see references in Goldsby and Kohlstedt (2001)); it is plausibly manifested in very low stress geological settings but has not yet been directly observed in ice in the laboratory.

Secondary phases introduce a complexity to deformation that depends not only on volume fractions and constitutive relationships of those phases, but also their spatial distribution and chemical reactivity with the primary phase. The effect on ice flow behavior of inert materials such as hard particulates is well understood at high and low temperatures (Baker and Gerberich, 1979; Durham et al., 1992, 2009; Hooke et al., 1972; Mangold et al., 2002). However, systems of ice and secondary phases exhibiting a eutectic are far less predictable, owing to weak heterophase interfaces (at $T^* \sim T_e$) and the presence of a melt phase ($T > T_e$) that may enhance grain boundary processes.

Creep tests on partially molten aggregates of saline ice by De La Chapelle et al. (1995, 1999) revealed low $n = 1.8 \pm 0.2$ behavior in the low-stress portion of the dislocation creep regime of pure ice—consistent with an enhanced rate of GBS. Hirth and Kohlstedt (1995) observed similar weakening in partially molten dunites, and argued that grain boundary diffusion and GBS were contributing more to deformation than activity of the stronger slip systems of olivine.

The enhancement of grain boundary processes in eutectic mixtures is expected at slightly subsolidus temperatures as well. McCarthy et al. (2011) found fine-scale ice-meridianiite ($MgSO_4 \cdot 11H_2O$) eutectic intergrowths to manifest a "colony boundary sliding" mechanism analogous to GBS in the range $0.85 < T/T_e < 0.93$. In general though, creep tests of ice-rich eutectic systems at subsolidus temperatures have not suggested enhancement of grain boundary processes, as most have been performed at relatively high stresses (De La Chapelle et al., 1995; Durham et al., 1993, 2005).

3. Experimental methods

Sample material of various compositions was fabricated by mixing measured amounts of granular ice (coarse-grained, $180 < d < 250$ μm; and in one case fine-grained, $2 < d < 10$ μm) with unsorted, finely powdered eutectic ice-MP6. The coarse-grained ice was ground and sieved, while the fine-grained ice was fabricated by rapid depressurization of the high-pressure ice II phase (Stern et al., 1997). In both cases the starting material was pore-free ice frozen from deionized water, deaerated by freezing from bottom to top, excluding gas ahead of the freezing front. The eutectic mixture itself was made by dissolving anhydrous $Mg(ClO_4)_2$ in water at a H_2O:$Mg(ClO_4)_2$ mass ratio of 56:44 (Fig. 1), then cooling below T_e. We determined degree of crystallinity of the frozen solid by X-ray diffraction (XRD) (Fig. 2, inset 3). Upon first cooling the solid is highly non-crystalline; it is also rather soft, with a consistency at 190–200 K of modeling clay. If T is cycled above and below T_e, the material devitrifies dramatically, and also becomes much harder. (Agitation during cooling assists devitrification.) At this stage the material is sufficiently hard and brittle that it can be pulverized for the purposes of sample fabrication. When the T-cycled material is further pressurized above 100 MPa at the start of a deformation run, it becomes completely crystalline, within the resolution limits of XRD. Fig. 2 also shows cryogenic scanning electron microscope images of an ice-MP6 eutectic that we deformed at high pressure (run 603). The eutectic solid has a texture that is fairly typical of other eutectics, displaying interfingering of extended zones of the two component phases, ice and MP6 (discussed below in the "Microstructural observations" subsection).

Compressional creep (i.e., constant stress) tests on composite specimens of ice and MP6 were performed under elevated confining pressure in the gas-medium, cryogenic triaxial deformation apparatus described by Heard et al. (1990). The purpose of confining pressure in this instance is not so much to simulate NPLD pressures (which are greatly exceeded here) as to suppress fracturing and assure martian-like ductile flow at laboratory strain rates, which are necessarily many orders of magnitude higher than in the NPLD. Cylindrical specimens approximately 25 mm in diameter and 60 mm in length were prepared by spooning mixed powders of desired composition into indium tubes, tamping lightly to remove large pores, then sealing the tubes to end plugs (Fig. 3a). All handling and storage was at 150 K or cooler. Once closed inside the deformation apparatus the sample was pressurized hydrostatically to 150 MPa for two reasons: to assure complete crystallinity, and

Table 1
Eq. (1) parameters for various creep mechanisms of ice I_h.

	log$A$[a]	n	p	E^* (kJ/mol)	V^* (cm^3/mol)	Source
Dislocation creep	5.1	4.0	0	61	−13	Durham et al. (1992)
Basal slip	7.7	2.4	0	60		Goldsby and Kohlstedt (2001)
GBS ($T < 255$ K)	−2.4	1.8	1.4	49		Goldsby and Kohlstedt (1997, 2001)
GBS ($T > 255$ K)	26.5	1.8	1.4	192		Goldsby and Kohlstedt (1997, 2001)

[a] For σ in MPa, d in μm.

Please cite this article in press as: Lenferink, H.J., et al. Weakening of ice by magnesium perchlorate hydrate. Icarus (2012), http://dx.doi.org/10.1016/j.icarus.2012.09.028

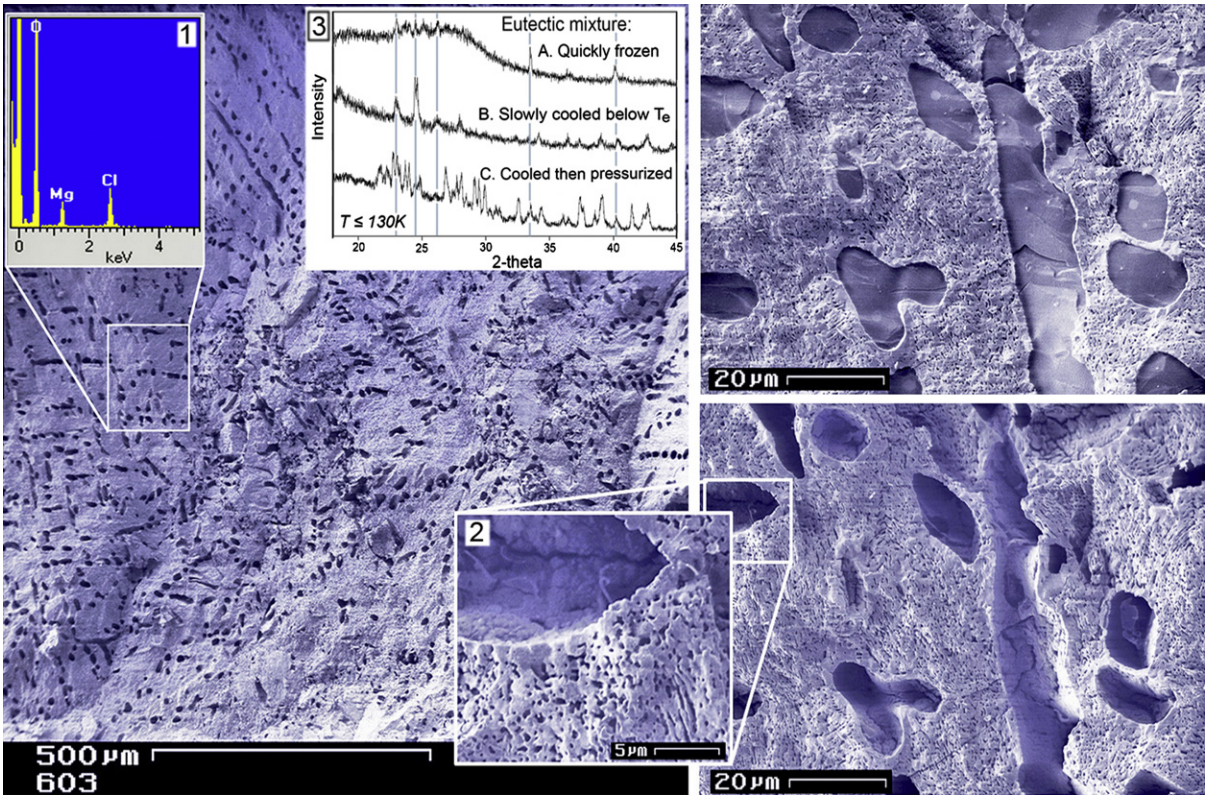

Fig. 2. Cryogenic SEM images of ice + Mg perchlorate hydrate (MP6) eutectic composition sample 603. Low-magnification CSEM image at left shows the MP6 phase after most of the ice has sublimated. Here, ice originally occupied the open channels and holes seen along the surface, with larger "pods" of ice distributed in a loosely uniform manner and typically spaced ~50 μm apart. Energy-dispersive X-ray scans of the remaining solid phase (inset 1) confirm oxygen, magnesium, and chlorine as the only measurable elements in the spectra in addition to hydrogen. Images at right show a section of sample after minor sublimation (top) and major sublimation (bottom) of the ice 20 min later. Many ice pods are isolated rather than interconnected below the surface. Detail of outlined box in lower right panel is shown in inset 2. Eutectic material was initially prepared by temperature cycling and slow cooling of the liquid phase below T_e followed by pressurization, as discussed in the text, and shown by cryogenic X-ray diffraction (XRD) to produce a more highly crystalline material than cooling only (inset 3; compare lower XRD scan C to upper and middle scans A and B. Vertical lines locate H_2O ice peaks.).

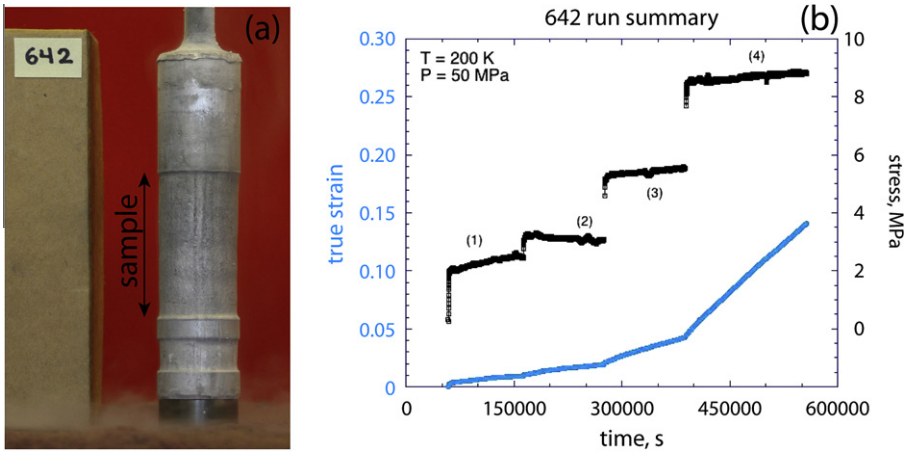

Fig. 3. Sample assembly for run 642, coarse grained ice with MP6 volume fraction $X_{MP6} = 0.10$. (a) Appearance of sample following a strain of about 0.17. For scale the darker disk at the bottom has a diameter of 25.4 mm. The deformation sample occupies the 45-mm length of reduced diameter in the central portion of the assembly. The sample is bounded top and bottom by steel end caps. All parts are sealed inside a tube of indium metal of wall thickness 0.5 mm, which keeps the gas pressure medium from entering the sample and assures an effective mechanical confinement. The bottom end cap includes an annular chamber that is mechanically shielded from the differential load, allowing comparison of deformed and undeformed material subjected to precisely the same temperature, pressure, and exposure time. A portion of the internal force gage extends from the top of the upper plug. (b) Run record for run 642 showing strain (blue, lower) and differential stress (black, upper) as a function of time. There were four steps in this run at four nominally constant levels of stress. Axial load is constantly adjusted upwards during the run to maintain constant stress as cross-sectional area of the sample increases. The adjustment is based on an estimate of real-time sample area. More exact post-test measurement of final sample area is then used to correct estimated real time area, and the slight slope to the stress curves at each step reflects this correction. The nonlinear relationship between stress and the rate of change of strain ($n \approx 3$ in Eq. (1)) is apparent in the four steps. (For interpretation of the references to color in this figure legend, the reader is referred to the web version of this article.)

Please cite this article in press as: Lenferink, H.J., et al. Weakening of ice by magnesium perchlorate hydrate. Icarus (2012), http://dx.doi.org/10.1016/j.icarus.2012.09.028

Table 2
Experimental conditions and results.

Run (step)	X_{MP6}	T (K)	σ (MPa)	ε	$\dot{\varepsilon}$ (s^{-1})
603(1)	0.47	180	18.0	0.026	5.26×10^{-7}
603(2)		190	5.5	0.073	1.14×10^{-6}
603(3)		195	3.0	0.116	2.00×10^{-6}
635	0	200	30.4	0.351	4.10×10^{-5}
637(1)[a]	0.10	189	8.4	0.051	6.03×10^{-7}
637(2)		199	5.9	0.079	3.72×10^{-7}
637(3)		210	3.2	0.116	2.25×10^{-5}
637(4)		210	3.9	0.176	5.23×10^{-5}
638(1)	0.05	190	25.6	0.062	1.16×10^{-5}
638(2)		190	18.6	0.094	3.17×10^{-6}
638(3)		190	14.6	0.112	1.19×10^{-6}
638(4)		200	4.8	0.142	2.78×10^{-7}
638(5)		200	10.2	0.166	1.05×10^{-6}
638(6)		200	14.6	0.192	3.85×10^{-6}
638(7)		200	12.6	0.212	2.13×10^{-6}
638(8)		200	18.9	0.241	1.06×10^{-5}
639[c]	0.02, 0	190	23.9	0.301	1.25×10^{-6}
640(1)	0.10	210	4.2	0.064	5.20×10^{-6}
640(1)		210	4.2	0.064	7.14×10^{-6}
640(2)[b]		200	8.4	0.078	2.34×10^{-7}
640(2)[b]		200	8.4	0.103	1.53×10^{-7}
640(3)[b]		210	4.2	0.179	4.42×10^{-7}
641(1)[a]	0.10	200	5.4	0.059	1.44×10^{-6}
641(2)		200	2.3	0.082	7.15×10^{-8}
641(3)		200	2.1	0.101	5.59×10^{-8}
642(1)	0.10	200	2.4	0.011	5.06×10^{-8}
642(2)		200	3.1	0.023	7.20×10^{-8}
642(3)		200	5.4	0.051	2.12×10^{-7}
642(4)		200	8.6	0.171	6.69×10^{-7}
643(1)	0.02	200	5.6	0.029	1.04×10^{-7}
643(2)		200	8.5	0.063	1.94×10^{-7}
643(3)		200	11.1	0.089	4.43×10^{-7}
643(4)		200	14.4	0.170	1.20×10^{-6}
657(1)	0.02	200	2.9	0.022	7.13×10^{-8}
657(2)		200	3.9	0.045	1.48×10^{-7}
657(3)		200	5.0	0.070	2.55×10^{-7}
657(4)		200	6.4	0.108	3.59×10^{-7}

[a] Affected by transient deformation of sample assembly; not plotted in Fig. 4.
[b] Lower-T steps following a 210-K step not plotted in Fig. 4; melt segregation suspected.
[c] Assembly of two vertically (along σ axis) stacked cylinders of the two X_{MP6} listed.

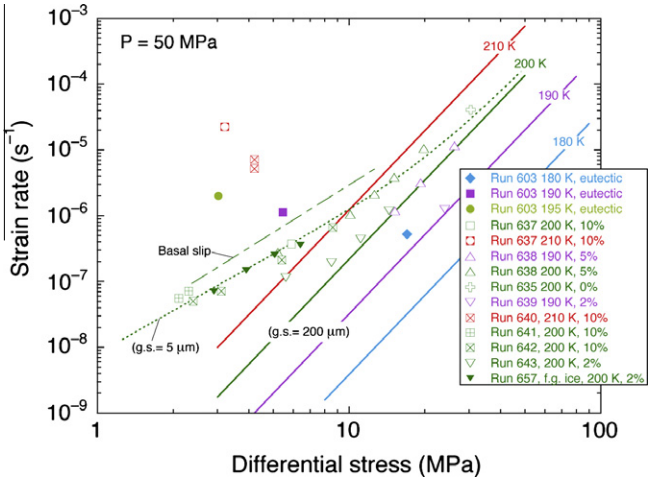

Fig. 4. Data from Table 2 plotted as log $\dot{\varepsilon}$ vs. log σ. Temperature and MP6 content are coded by symbol color and shape, respectively. Different runs are distinguished by different decorations within symbols. In one case small inverted triangles vs. large inverted triangles refer to fine-grained and coarse-grained ice matrix, respectively. Measurement uncertainty in stress and strain rate is approximately equal to the size of the data points. Not plotted are data from steps in which the sample was initially misoriented relative to the loading piston, as well as points at $T \leqslant 200$ K for which $T = 210$ K had previously been encountered (as melt segregation likely occurred). Shown for comparison are creep curves for coarse- (200 μm) and fine-grained (5 μm) ice, calculated using the flow parameters in Table 1. (For interpretation of the references to color in this figure legend, the reader is referred to the web version of this article.)

to squeeze out all sample porosity that would otherwise interfere with the mechanical response to the applied shape-changing stress. Runs consisted of deformation steps at various stress and temperature conditions, and were all performed at a gas confining pressure of 50 MPa. An example of a stepping test is shown in Fig. 3b. Samples were shortened by a total of 10–30% over a period of hours to days, depending on conditions.

The step-testing technique has the advantage of yielding several data points per run, but the disadvantage of potentially overlooking subtle but important strain-dependent effects. The immediate strain-rate response to a change in environmental conditions at the beginning of a step is usually transient (i.e., strain-dependent). When the sample appears to have reached approximate steady state behavior, the current strain rate becomes the tabulated strain rate for that step. For the purposes of a reconnaissance investigation we assume that further strain dependence does not exist—an assumption that must eventually be confirmed by experiment.

Cryogenic scanning electron microscopy (CSEM) was used to observe the grain sizes and phase distribution of all samples in this study. Samples were shipped and prepared for CSEM at temperatures below ~85 K, then transferred to a cryo-preparation station (Gatan Alto 2100) in which each sample was cleaved under vacuum to produce fresh surfaces uncontaminated by water condensation. Samples were then transferred directly into a LEO982 field-emission SEM. A thermocouple embedded in the SEM sample stage monitored temperature throughout the imaging process. Images were taken at $T < 85$ K and vacuum below 10^{-5} mbar.

4. Results and analysis

4.1. Creep results

Test conditions and creep results are given in Table 2. We tested ten samples of MP6 volume fraction $0 \leqslant X_{MP6} \leqslant 0.47$ at $180 \leqslant T \leqslant 210$ K in stepped tests that yielded 32 data points. One of the ten (639), a single-condition test, was a stacked assembly designed for a comparative measurement of $X_{MP6} = 0.02$ ice and coarse-grained pure ice. As stated in the previous section, the ice component in one of the nine mixtures (657) was fine- rather than coarse-grained. After discovering a strong effect of MP6 on strength and seeing signs of partial melt at 210 K (see below), we concentrated mostly on lower temperatures, predominantly 200 K, and on MP6 concentrations $X_{MP6} \leqslant 0.10$. The 32 data points are plotted in Fig. 4 along with temperature contours for the creep of polycrystalline ice of coarse-grained (Durham et al., 1992) and 5-μm grain size (Goldsby and Kohlstedt, 2001).

The effect of MP6 on the ductile strength of ice is profound. All test specimens were less viscous than pure, coarse-grained ice at the same stress and temperature conditions. At 180 K the eutectic alloy $X_e = 0.47$ is nearly 1.5 orders of magnitude less viscous than pure ice at the same temperature, and at 195 K the viscosity contrast is well over 10^3. For samples of $X_{MP6} \leqslant 0.10$, Fig. 4 shows two distinct rheological regimes: above $\sigma = 10$ MPa, log strain rate vs. log stress for a given concentration and temperature follows a slope $n \approx 4$ (Eq. (1)), which parallels that of pure ice in dislocation creep. Below 10 MPa, the data follow more closely the $n \approx 2$ trend of grain-size sensitive mechanisms seen in pure ice (Goldsby and Kohlstedt, 2001). The effect of concentration on strength may be

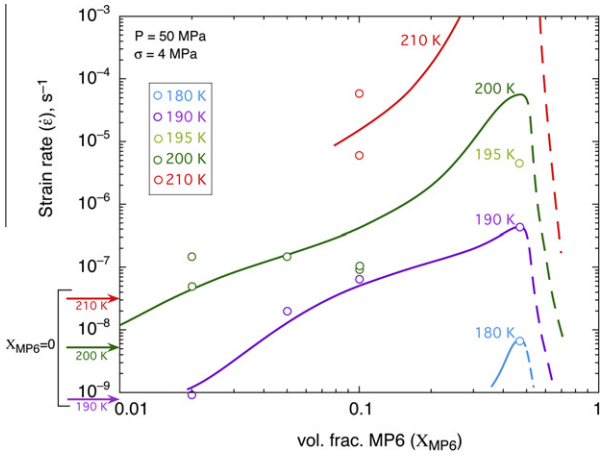

Fig. 5. Data from Fig. 4 replotted as log strain rate vs. X_{MP6} at fixed $\sigma = 4$ MPa, emphasizing the weakening effect of MP6. Strain rate is extrapolated as necessary to the 4 MPa value on the basis of $n = 2$ or 4 in Eq. (1), depending on the trend in Fig. 4. Symbol shapes have different meaning from Fig. 4, but color coding is the same. Curves are drawn by hand as estimated fits, without consideration of specific physical mechanism. The double inflection points appearing in the 190-K curve and implied in the 200-K curve suggest complexity in the physics. Arrows on the vertical axis indicate strain rates for pure ice at the three temperatures indicated. The horizontal axis is logarithmic to bring out detail rather than to imply a physical mechanism. Note that if plotted on a linear scale, the drop in strain rate (i.e., increase in strength) to the right of the peak at the eutectic composition would appear less precipitous than the one to the left of the peak. The curves to the right of the peak (dashed) are speculative and their locations are based mainly on the fact that the melting point of MP6 is well over 100 K higher than that of ice. The strain rate enhancement factor with respect to pure ice is well in excess of an order of magnitude even at relatively low X_{MP6}, and the factor increases with increasing temperature. (For interpretation of the references to color in this figure legend, the reader is referred to the web version of this article.)

more pronounced in the $n \approx 4$ regime than in the $n \approx 2$ regime: there is a relatively small spread in strengths among the mixtures as they curve with decreasing σ from the high to the low n regime. It is not surprising that the one mixture involving fine-grained ice (small inverted triangles in Fig. 4) follows the $n \approx 2$ trend at $\sigma < 10$ MPa since that is the expected behavior of pure, fine-grain ice (short dashed line in Fig. 4). What is remarkable is that coarse-grained ice containing a relatively small amount of MP6 behaves rheologically like fine-grained ice. The behavior of this group of samples shows a rheological similarity to basal slip in single crystal ice: it not only has a strength in this same general region (long-dashed line in Fig. 4), but like basal slip is also insensitive to grain size. This point is discussed below in more detail.

The data viewed as strain rate vs. X_{MP6} at constant stress and temperature show more clearly the magnitude of the weakening effect of MP6 (Fig. 5). Data are sparse and somewhat scattered, but for the most part consistently indicate that the profound weakening near X_e continues to very low X_{MP6}. The best resolved measurement is that of the stacked assembly run 639, conducted at 190 K, which showed on the basis of comparative shape change a strain rate enhancement in $X_{MP6} = 0.02$ ice with respect to pure ice by a factor of 1.16 ± 0.04. Evidently strain rate enhancement over pure ice increases with temperature above 190 K, and if the estimated trends in Fig. 5 correctly characterize this behavior, there will continue to be significant strain enhancement at 200 K and above even for $X_{MP6} < 0.01$.

4.2. Partial melting

The two samples deformed at 210 K show almost unmistakable signs of having partially melted. Firstly they exhibited a viscosity drop between 200 and 210 K that was anomalously high given the temperature sensitivity of the viscosity of MP6 mixtures (and of pure ice) at lower temperatures (Fig. 5). Secondly, and more convincingly, both samples lost volume during the experiments. External dimensions indicated volume loss, and a rigid ~ 1 cm^3 internal plenum, which ordinarily remains empty during a deformation test, was filled with material that in one case was confirmed by density measurement to be of eutectic composition. The plenum communicates gas pressure with the sample through an axial hole 0.5 mm in diameter by 20 mm in length; the plenum is vented to atmosphere through a much finer axial hole in the force gage (i.e., inside the tube extending from the top of the assembly shown in Fig. 3a). We cannot say at this point how much, if any, material escaped through the vent hole, or if the Clapeyron slope for eutectic melting is sufficiently negative that material resolidified upon entering the plenum. In any case, the material in the plenum was solid when viewed because the sample assembly cooled to 77 K before it was taken apart. The Clapeyron slope for melting of ice I is approximately -10 MPa/K; if that value has any relationship to the value for eutectic melting, then given the 50-MPa pressure drop between sample and plenum, our observation of melt formation at 210 K does not better constrain the $P = 0$ melting point relative to previously published work (Chevrier et al., 2009; Pestova et al., 2005; Stillman and Grimm, 2011b).

4.3. Microstructural observations

Sections from all samples were observed by CSEM. The sample of eutectic composition $X_{MP6} = 0.47$ (Fig. 2) exhibits many regions with classic eutectic solidification microstructures similar to those described by McCarthy et al. (2007), in which the hydrate phase forms a matrix around regularly spaced rods of ice I. Also similar to the McCarthy et al. (2007) work was the observation of rapid sublimation of the ice phase in all samples, in contrast to the behavior of pure ice samples that sublimate very slowly in the FE-SEM at comparable conditions. The sublimation effect is illustrated in the right-hand panels of Fig. 2, which span a 20-min interval.

Figs. 6–8 show images from samples of $X_{MP6} = 0.10$, 0.05, and 0.02, respectively. The general appearance of ice grains rimmed by MP6 was consistently found throughout all mixed-phase samples, demonstrating the excellent reproducibility of phase distribution that in turn supports comparison of run results. In the absence of rigorous microanalysis of individual grains in these samples, we assume that the ice grains have little or no MP6 in their interiors, which is consistent with close inspection of the SEM images (e.g., Fig. 6c). Quantifying the amount of ice present in the grain boundary matrix material is difficult, but comparison of the eutectic solid in Fig. 2 and the phase in wider grain boundaries in Figs. 6–8 indicates that the intergranular material is predominantly MP6. While much of the MP6 phase appears pitted and/or riddled with small cracks, these are largely an artifact of the high-vacuum conditions in the SEM column. This is illustrated by the time-lapse sequence shown in Fig. 7b and c: the early view (b) shows the relatively dense substrate of the MP6 phase, compared to its appearance 25 min later (c) where not only has the ice sublimated, but the surface of the MP6 has degraded as well.

At $X_{MP6} = 0.10$ and 0.05 (Figs. 6 and 7), the coating of ice grains by MP6 is complete—there are few, if any, direct grain-to-grain ice contacts. Distribution of MP6 in the $X_{MP6} = 0.02$ is sometimes more heterogeneous, although it still typically surrounds the ice grains (Fig. 8). At this point we cannot rule out the possibility that the heterogeneity is a mixing problem, so it is difficult to comment on rheological effects. Nonetheless, the similarity in overall phase distribution of the $X_{MP6} = 0.02$ samples in Fig. 8 (643 vs. 657) is striking: both show 100–300 μm diameter grains or domains of ice, even though those in 657 are domains composed of fine-

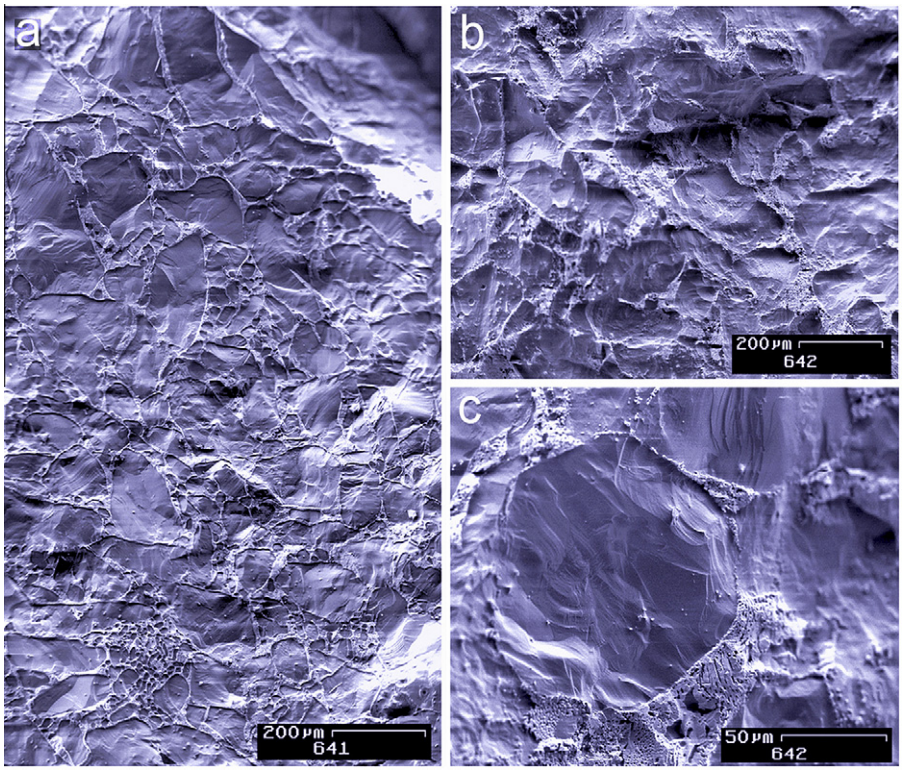

Fig. 6. CSEM comparison of two different $X_{MP6} = 0.10$ samples showing the overall textural uniformity within a single sample (panel a, sample 641) as well as between samples (compare 641 in panel a with 642 in panel b). MP6 is concentrated in the light shaded material standing high in relief relative to the grains of ice that it surrounds. A single representative ice grain from sample 642 is enlarged in c, showing it to be essentially free of MP6 inclusions.

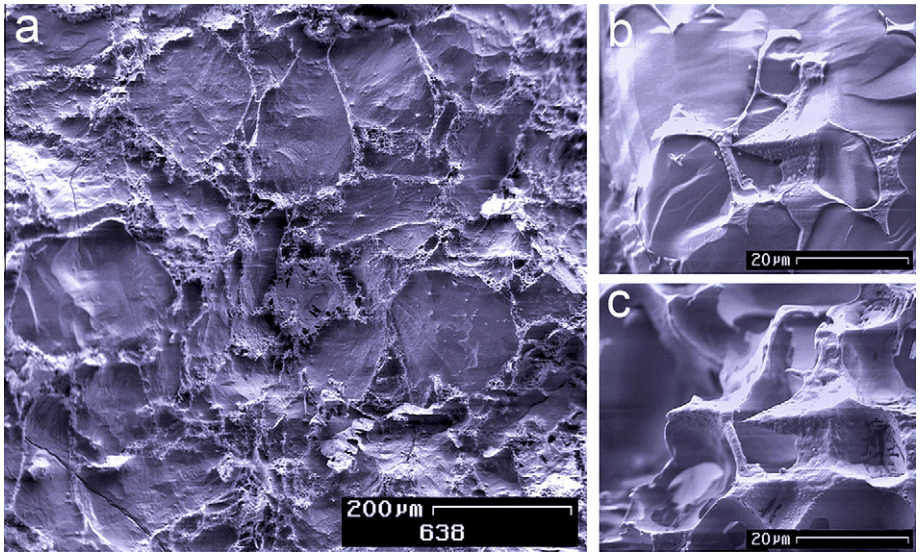

Fig. 7. (a) CSEM image of sample 638, $X_{MP6} = 0.05$, showing ice grains uniformly coated by MP6-rich material. Despite the lower MP6 content here compared to Fig. 6, it appears quite pronounced due to the time the sample spent in the high-vacuum SEM chamber and the accompanying sublimation of ice. Panels (b) and (c) show a 25-min time lapse sequence of an identical section of sample, illustrating the dramatic change that accompanies sublimation of the ice as well as surface damage of MP6.

grained ice rather than larger single grains. We observe thicker rims of MP6 in samples containing higher concentrations, although the faster sublimation of ice with respect to MP6 can sometimes exaggerate the apparent MP6 content.

The fine-grained $X_{MP6} = 0.02$ sample gives tantalizing clues about the kinetics of textural equilibration. Evidently the preponderance of the MP6 in this sample is on the domain boundaries, but on close examination of Fig. 8b, one sees a fine web of bright ridges extending from the domain boundaries a few tens of microns into the domains. Presumably the system is evolving in the direction of textural equilibrium, with MP6-rich material moving from the domain boundaries to coat the boundaries between individual ice grains. Fig. 9 shows closer views of these edges of the ice domain that solidly support this interpretation.

Similarities in geologically relevant materials to the microstructures seen here include the texture of wetting fluids (water, liquid

Please cite this article in press as: Lenferink, H.J., et al. Weakening of ice by magnesium perchlorate hydrate. Icarus (2012), http://dx.doi.org/10.1016/j.icarus.2012.09.028

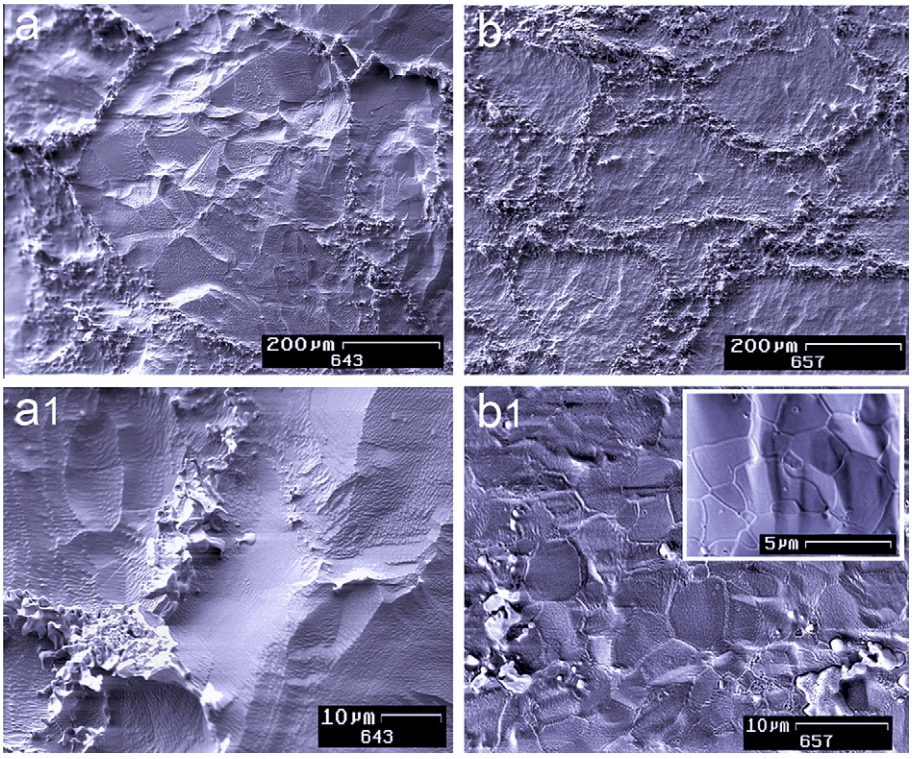

Fig. 8. CSEM comparison of X_{MP6} = 0.02 samples 643 (made with coarse grained ice) and 657 (made with fine-grained ice) in panels (a) and (b) respectively. The upper images show low magnification images of the overall sample structure, and the lower photos (a1, b1) detail ice sections from each sample. As expected, no ice-to-ice grain boundaries are visible in coarse-grained 643 (a1) whereas grain boundaries are clearly visible in fine-grained 657 (b1 and inset). The high-standing MP6-rich material in (a1) is at an ice grain boundary, not interior within the ice. In comparison, sample 657 often exhibits small amounts of MP6 within the ice domains (b1), although many sections of any given domain show ice-on-ice grain contacts with no MP6 (b1 inset). Ice grain size in 657 is fairly uniform at several microns in diameter (b1 and inset).

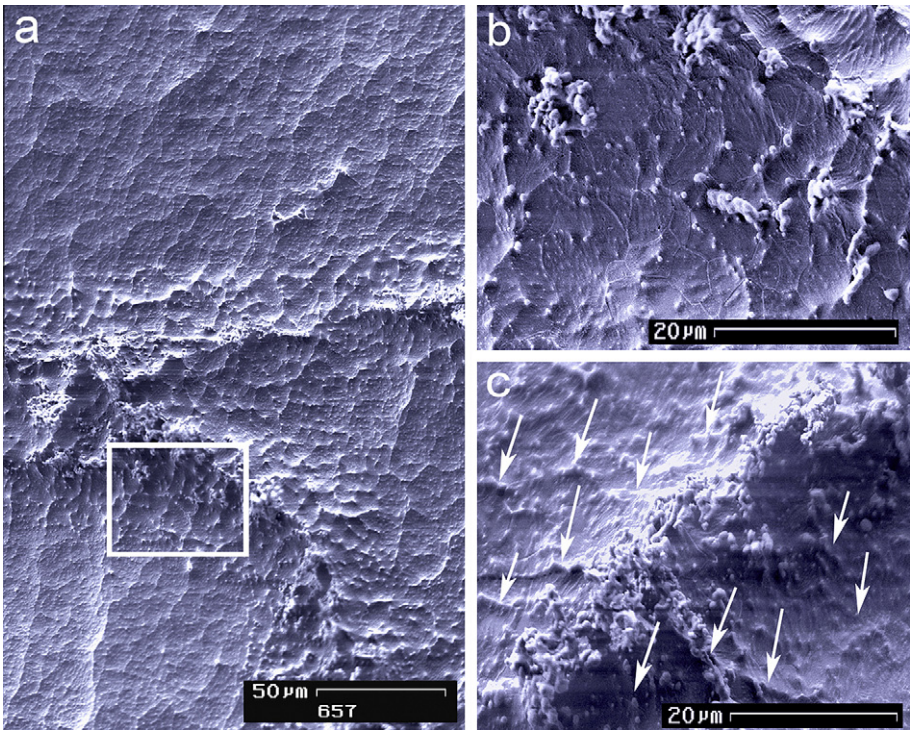

Fig. 9. (a) Overview of a domain boundary from the center of sample 657 (Fig. 8, right column) showing apparent "wicking" of MP6-rich material into the fine-grained ice. The clear gradient in MP6 concentration away from the boundary is best seen at this scale. (b) Enlargement of box outlined in (a), showing ice grain boundaries at several microns in diameter. The MP6 is unstable under extended exposure to the electron beam and tends to collect into the small spheres and clusters of spheres seen here. Virtually all MP6 lies along visible ice grain boundaries. (c) Similar features in a different portion of the sample, with arrows indicating several ridge-like structures where MP6-rich material appears to be wicked or drawn away from the domain boundary.

Please cite this article in press as: Lenferink, H.J., et al. Weakening of ice by magnesium perchlorate hydrate. Icarus (2012), http://dx.doi.org/10.1016/j.icarus.2012.09.028

CO_2, partial melts) in polycrystalline rocks where the dihedral angle between fluid and matrix, driven by relative surface energies (capillary forces), is very low (Ketcham and Hobbs, 1969; Kohlstedt, 2002). If the textural control of the MP6-rich grain boundary phase in our samples is analogous to that for grain-boundary melts, then given its propensity to completely surround ice grains even at low volume fractions, the ice-MP6 grain boundary dihedral angle θ must be nearly zero.

However, there are two reasons to believe the analogy to fluids in rocks may not be valid in the ice-MP6 system. The first is the lack of any sign of capillary forces affecting the kinetics of the development of textural equilibrium, in particular the lack of isolated pockets of MP6 forming at three-grain junctions or thickening of thinnest MP6 layers along a significant fraction of three-grain junctions in our samples. Fig. 8b is particularly telling in this regard: three-grain ice junctions are plainly visible as are small spheroidal masses of MP6 formed from sublimation and other surface damage processes incurred directly under the electron beam. The spheres appear to lie along grain boundaries, presumably since they are derived from grain boundary material left after ice sublimation, yet there is no clear preference for their occurrence at three-grain junctions. If capillary forces alone drive texture, then the fluid should first appear in three-grain junctions, where grain radii (and therefore ice surface energies) are highest. To the extent that a rock-fluid system of $\theta = 0$ has reached textural equilibrium, this effect may become less pronounced, but in our samples the heterogeneity of the $X_{MP6} = 0.02$ sample suggests they are not equilibrated, yet we see little sign that the MP6 layer is thicker at three-grain junctions than at two-grain junctions (i.e., grain faces). The second reason we suspect something other than capillary forces are at work is that our MP6 material is in fact a crystalline solid. According to our measurements, the eutectic composition is weak, but still distinctly non-liquid-like even at 200 K (green curve in Fig. 5).

5. Discussion

Although this investigation is preliminary and measurement uncertainties are accordingly large, two unusual phenomena are apparent: a profound mechanical weakening associated with the presence of small amounts of MP6, and a remarkable—considering that the material has been entirely below T_e—texture of ice grains surrounded partially or completely by MP6-rich material in the deformed samples. These two independent observations invite speculation about a causal relationship. If such a relationship exists, the morphology of the MP6-rich grain coating suggests a weakening associated with grain boundaries. The MP6-rich material may act in some way to mechanically weaken the connection between adjacent ice grains, either via (1) normal displacement, by removing contact points in the manner of pressure solution, or (2) shear displacement, by decreasing the friction between flat surfaces or by smoothing asperities between rough surfaces.

Diffusional flow tends to follow a linear stress–strain rate relationship and can probably be eliminated as a rate-limiting mechanism. But the mutual accommodation of intergranular shear displacement (in the form of GBS) and intragranular plasticity could account for this weakening and explain the rheological similarity to pure, fine-grained ice. Our creep results at stresses <10 MPa for $X_{MP6} = 0.05$ and 0.10 exhibit both the $n \approx 2$ dependence and level of strain rate of basal slip-limited creep, as seen in pure ice of grain size <5 μm (Goldsby and Kohlstedt, 1997, 2001). Perhaps, then, the presence of the MP6-rich material allows large ice grains to effectively act as if they were smaller.

The one grain size comparison we have, ~200 μm vs. ~5 μm at $X_{MP6} = 0.02$ and 200 K (runs 643 and 657), indicates a weak but non-zero grain-size dependence that may indicate a transitioning to GBS-limited creep at the conditions of the coarse-grained sample 643. Ordinarily grain-size dependence in GBS is more pronounced than that exhibited by 643 vs. 657. Therefore we might consider the possible effect of a fixed volume of MP6: if the thickness of the grain boundary layer matters in some way for the weakening effect, an increase in grain boundary area per unit volume, which enhances GBS in pure ice, would be offset by the thinning of the grain boundary layer with decreasing grain size.

6. Implications for ice flow in the North Polar Layered Deposits

Although the presence of perchlorate has only been confirmed at the Phoenix landing site (68.3°N, 127.0°W) in Vastitas Borealis (Hecht et al., 2009), modeling by Navarro-González et al. (2010) suggests that the Viking landers also detected perchlorate in Chryse Planitia (22.7°N, 48.2°W) and Utopia Planitia (48.3°N, 226.0°W). Given the pervasiveness of terrestrial perchlorate in hyperarid environments such as the Atacama Desert (Catling et al., 2010) and the Antarctic Dry Valleys (Kounaves et al., 2010), perchlorate is likely to be widespread in the martian polar regions, where it could potentially enhance flow rates within the Polar Layered Deposits.

Whether or not the topography and stratigraphy of the NPLD is consistent with past ice flow is currently a matter of debate. Winebrenner et al. (2008) analyzed the morphology of Gemina Lingula—a lobe of the NPLD—and demonstrated that its intertrough topography can be reproduced by glacial flow. Karlsson et al. (2011), however, concluded that the radar-detected subsurface stratigraphy of Gemina Lingula is inconsistent with the predictions of their flow modeling. In response, Winebrenner et al. (in preparation) showed that the stratigraphy of Gemina Lingula is not incompatible with a slope-dependent mass balance pattern, which they argue is more appropriate to the NPLD.

What is less contentious, though, is the widespread conclusion (Clifford et al., 2000; Greve and Mahajan, 2005; Hvidberg, 2003; Koutnik et al., 2012) that pure water ice at present-day NPLD thermal conditions (i.e., basal $T_b \sim 185$ K) is too viscous to undergo significant rates of flow. Koutnik et al. (2012) suggest that both warmer temperatures and flow enhancement (by at least a factor of 10) may be required to generate significant flow over plausible time scales. If our laboratory results can be extrapolated to low stresses and trace concentrations of MP6 ($\ll$1% by volume), then the presence of perchlorate in the NPLD could possibly provide the needed flow enhancement mechanism, particularly at slightly elevated basal temperatures ($190 < T_b < 210$ K). Such warming could potentially result from transient subsurface heating events or increased insolation at higher obliquities (Pathare and Paige, 2005). Moreover, if NPLD basal temperatures are elevated above the MP6 eutectic, then as Fisher et al. (2010) suggest, a perchlorate brine lubricated deformable bed may facilitate flow. A north polar flow hypothesis is therefore potentially plausible, and would be bolstered by the detection of perchlorate in the NPLD.

7. Conclusions

Mixtures of ice and MP6 are significantly weaker than pure ice at low stresses, and this weakening is most pronounced in material of eutectic composition. Specimens with 5% and 10% MP6 by volume exhibited low $n \approx 2$ behavior at stresses below 10 MPa, coinciding with the basal slip-limited creep of very fine-grained ice ($d = 5$ μm). A specimen with 2% MP6 by volume also exhibited low-n behavior at low stresses, coinciding with GBS-limited creep of ice with $d = 30$ μm. These observations of mixtures of ice and MP6 may be due to the weakening of ice grain boundaries by

Please cite this article in press as: Lenferink, H.J., et al. Weakening of ice by magnesium perchlorate hydrate. Icarus (2012), http://dx.doi.org/10.1016/j.icarus.2012.09.028

MP6, resulting in a mechanistic equivalence with pure, fine-grained ice. Future creep tests on ice plus MP6 will be aimed at (1) determining the critical MP6 content required for significant weakening; and (2) probing for grain size-sensitive regimes.

Based on this preliminary work, assumptions regarding flow in the NPLD should account for the weakening of ice by MP6 and the possibility of $n \approx 2$ behavior at martian stresses ($\sim$0.05 MPa: Zwally and Saba, 1999). If the results of our experiments can be extrapolated to low stresses and MP6 concentrations, then episodes of significant NPLD flow enhancement could result from the presence of perchlorate at slightly elevated basal temperatures.

Acknowledgments

The authors gratefully acknowledge support of NASA Mars Fundamental Research Grant Numbers NNX11AN37G and NNH12AT59I. H.J.L. acknowledges support of NASA Earth and Space Sciences Fellowship Number NNX11AP34H. We thank David Stillman, SWRI, Boulder, CO, for supplying us with our first MP6 material as well as with detailed and patient guidance on how to synthesize our own. Careful readings by S. Kirby and B. Kilgore (both USGS, Menlo Park) and two anonymous reviewers greatly improved this manuscript.

References

Baker, R.W., Gerberich, W.W., 1979. The effect of crystal size and dispersed-solid inclusions on the activation energy for creep of ice. J. Glaciol. 24, 179–194.

Catling, D.C. et al., 2010. Atmospheric origins of perchlorate on Mars and in the Atacama. J. Geophys. Res. 115, E00E11. http://dx.doi.org/10.1029/2009JE003425.

Chevrier, V.F., Hanley, J., Altheide, T.S., 2009. Stability of perchlorate hydrates and their liquid solutions at the Phoenix landing site, Mars. Geophys. Res. Lett. 36, L10202.

Clifford, S.M. et al., 2000. The state and future of Mars polar science and exploration. Icarus 144, 210–242.

De La Chapelle, S., Duval, P., Baudelet, B., 1995. Compressive creep of polycrystalline ice containing a liquid phase. Scripta Metall. Mater. 33, 447–450.

De La Chapelle, S., Milsch, H., Castelnau, O., Duval, P., 1999. Compressive creep of ice containing a liquid intergranular phase: Rate-controlling processes in the dislocation creep regime. Geophys. Res. Lett. 26, 251–254.

Durham, W.B., Kirby, S.H., Stern, L.A., 1992. Effects of dispersed particulates on the rheology of water ice at planetary conditions. J. Geophys. Res. – Planet. 97, 20883–20897.

Durham, W.B., Kirby, S.H., Stern, L.A., 1993. Flow of ices in the ammonia-water system. J. Geophys. Res. 98, 17667–17682.

Durham, W.B., Pathare, A.V., Stem, L.A., Lenferink, H.J., 2009. Mobility of icy sand packs, with application to martian permafrost. Geophys. Res. Lett. 36, L23203. http://dx.doi.org/10.1029/2009GL040392.

Durham, W.B., Stern, L.A., Kubo, T., Kirby, S.H., 2005. Flow strength of highly hydrated Mg- and Na-sulfate hydrate salts, pure and in mixtures with water ice, with application to Europa. J. Geophys. Res. – Planet. 110, E12010. http://dx.doi.org/10.1029/2005JE002475.

Fisher, D.A., Hecht, M.H., Kounaves, S.P., Catling, D.C., 2010. A perchlorate brine lubricated deformable bed facilitating flow of the north polar cap of Mars: Possible mechanism for water table recharging. J. Geophys. Res. – Planet. 115, E00E012.

Goldsby, D.L., Kohlstedt, D.L., 1997. Grain boundary sliding in fine-grained ice I. Scripta Mater. 37, 1399–1406.

Goldsby, D.L., Kohlstedt, D.L., 2001. Superplastic deformation of ice: Experimental observations. J. Geophys. Res. 106, 11017–11030.

Greve, R., Mahajan, R.A., 2005. Influence of ice rheology and dust content on the dynamics of the north-polar cap of Mars. Icarus 174, 475–485.

Heard, H.C., Durham, W.B., Boro, C.O., Kirby, S.H., 1990. A triaxial deformation apparatus for service at $77 \leqslant T \leqslant 273$ K. In: The Brittle–Ductile Transition in Rocks. Geophysical Monograph, vol. 56. American Geophysical Union, Washington, DC, pp. 225–228.

Hecht, M.H. et al., 2009. Detection of perchlorate and the soluble chemistry of martian soil at the Phoenix Lander site. Science 325, 64–67.

Hirth, G., Kohlstedt, D.L., 1995. Experimental constraints on the dynamics of the partially molten upper mantle: Deformation in the diffusion creep regime. J. Geophys. Res. – Sol. Earth 100, 1981–2001.

Hooke, R.L., Dahlin, B.B., Kauper, M.T., 1972. Creep of ice containing dispersed fine sand. J. Glaciol. 11, 327–336.

Hvidberg, C.S., 2003. Relationship between topography and flow in the north polar cap on Mars. Ann. Glaciol 37, 363–369.

Karlsson, N.B., Holt, J.W., Hindmarsh, R.C.A., 2011. Testing for flow in the North Polar Layered Deposits of Mars using radar stratigraphy and a simple 3D ice-flow model. Geophys. Res. Lett. 38, L24204.

Ketcham, W.M., Hobbs, P.V., 1969. An experimental determination of the surface energies of ice. Philos. Mag. 19, 1161–1173.

Kohlstedt, D.L., 2002. Partial melting and deformation. In: Karato, S., Wenk, H.R. (Eds.), Plastic Deformation of Minerals and Rocks, pp. 121–135.

Kounaves, S.P. et al., 2010. Discovery of natural perchlorate in the Antarctic Dry Valleys and its Global Implications. Environ. Sci. Technol. 44, 2360–2364.

Koutnik, M.R., Waddington, E.D., Winebrenner, D.P., Pathare, A.V., 2012. Response timescales for martian ice masses and implications for ice flow on Mars. Icarus, this issue.

Langevin, Y., Poulet, F., Bibring, J.P., Gondet, B., 2005. Sulfates in the north polar region of Mars detected by OMEGA/Mars express. Science 307, 1584–1586.

Mangold, N., Allemand, P., Duval, P., Geraud, Y., Thomas, P., 2002. Experimental and theoretical deformation of ice-rock mixtures: Implications on rheology and ice content of martian permafrost. Planet. Space Sci. 50, 385–401.

McCarthy, C., Cooper, R.F., Goldsby, D.L., Durham, W.B., Kirby, S.H., 2011. Transient and steady state creep response of ice I and magnesium sulfate hydrate eutectic aggregates. J. Geophys. Res. – Planet. 116, E04007. http://dx.doi.org/10.1029/2010je003689.

McCarthy, C., Cooper, R.F., Kirby, S.H., Rieck, K.D., Stern, L.A., 2007. Solidification and microstructures of binary ice-I/hydrate eutectic aggregates. Am. Mineral. 92, 1550–1560.

Navarro-González, R., Vargas, E., de la Rosa, J., Raga, A.C., McKay, C.P., 2010. Reanalysis of the viking results suggests perchlorate and organics at midlatitudes on Mars. J. Geophys. Res. 115, E12010. http://dx.doi.org/10.1029/2010JE003599.

Pathare, A.V., Paige, D.A., 2005. The effects of martian orbital variations upon the sublimation and relaxation of north polar troughs and scarps. Icarus 174, 419–443.

Pestova, O.N., Myund, L.A., Khripun, M.K., Prigaro, A.V., 2005. Polythermal study of the systems M(ClO_4)(2)-H_2O (M^{2+} = Mg^{2+}, Ca^{2+}, Sr^{2+}, Ba^{2+}). Russ. J. Appl. Chem. 78, 409–413.

Poirier, J.-P., 1985. Creep of Crystals. Cambridge University Press, New York.

Robertson, K., Bish, D., 2011. Stability of phases in the Mg(ClO(4))(2)·nH(2)O system and implications for perchlorate occurrences on Mars. J. Geophys. Res. – Planet. 116, E07006. http://dx.doi.org/10.1029/2010JE003754.

Stern, L.A., Durham, W.B., Kirby, S.H., 1997. Grain-size-induced weakening of H_2O ices I and II, and associated anisotropic recrystallization. J. Geophys. Res. – Sol. Earth 102, 5313–5325.

Stillman, D.E., Grimm, R.E., 2011a. Dielectric signatures of adsorbed and salty liquid water at the Phoenix landing site, Mars. J. Geophys. Res. – Planet. 116, E09005. http://dx.doi.org/10.1029/2011JE003838.

Stillman, D.E., Grimm, R.E., 2011b. Heterogeneous adsorbed and salty liquid water at the Phoenix landing site, Mars. Lunar Planet. Sci. XLII. Abstract #2578.

Winebrenner, D.P., Koutnik, M.R., Waddington, E.D., Pathare, A.V., Murray, B.C., Byrne, S., Bamber, J.L., 2008. Evidence for ice flow prior to trough formation in the martian North Polar Layered Deposits. Icarus 195, 90–105.

Zent, A.P. et al., 2010. Initial results from the thermal and electrical conductivity probe (TECP) on Phoenix. J. Geophys. Res. – Planet. 115, E00E14. http://dx.doi.org/10.1029/2009JE003420.

Zwally, H.J., Saba, J.L., 1999. Driving stresses in Mars polar ice caps and conditions for ice flow. Int. Conf. Mars V. Abstract #971.